

# Square-Section Tube-Concrete Structures Studying Under Axial Compression Both with Spiral Reinforcement of the Concrete Core and Without Reinforcement



Vladimir Rimshin , Anatoly Krishan , Elena Korol ,  
Svetlana Roshchina , and Igor Shubin 

**Abstract** The article contains a research methodology and the experiments results on samples of square-section tube-concrete structures, both with spiral reinforcement of the concrete core, and without reinforcement, which perceive a short-term compressive load. The aim was studying the strength and features of the stress–strain state of square-section tube-concrete structures samples, made of concrete of classes B40 and B80, taking into account their flexibility. The experimental part of the work was carried out using modern equipment and devices certified and metrologically certified. Probabilistic-statistical calculation methods were used to process the array of experimental data obtained. According to the requirements of the current regulatory documents, before the tests, the measurement error assessment by the tensoresistive method was carried out. The features of force resistance revealed in experiments testify to the operation of a concrete core and a steel tube under conditions of a volumetric stress state. The deformation nature of the steel tube suggests that its walls experience not only compression in the axial direction. Stretching and bending of the walls from the lateral pressure of the concrete core is also observed. Thus, the tube contribution to the perception of the force  $N_u^{exp}$  is significantly less

---

V. Rimshin (✉) · E. Korol

Moscow State University of Civil Engineering (MGSU), Yaroslavskoye Shosse, 129337, 26,  
Moscow, Russia

e-mail: [v.rimshin@niisf.ru](mailto:v.rimshin@niisf.ru)

V. Rimshin · I. Shubin

Research Institute of Building Physics of the Russian Academy of Architecture and Building  
Sciences, 21, Locomotive Passage, 127238 Moscow, Russia

A. Krishan (✉)

Nosov Magnitogorsk State Technical University, 455000, 38, Lenin Avenue, Magnitogorsk,  
Russia

e-mail: [kris\\_al@mail.ru](mailto:kris_al@mail.ru)

S. Roshchina

Vladimir State University Named After A.G. and N.G.Stoletov, 87Gorky Street, 600000 Vladimir,  
Russia

than it would be in the assumption of its operation in uniaxial compression. It indicates a noticeably greater contribution of concrete to the perception of the force  $N_{it}^{exp}$  in comparison with the conditions of uniaxial compression. The main conclusion of the experiments follows from it. It is advisable to increase the strength of square-section tube-concrete structures by using high-strength concrete and providing more effective indirect reinforcement for it. The power resistance features of square-section tube-concrete structures revealed in the experiments must be taken into account when calculating their strength.

**Keywords** Tube-concrete elements of square cross section · Spiral reinforcement · Axial compression · Tensorresistor method · Force resistance

## 1 Research Methods

The object of the experimental study were samples of square-section tube-concrete structures, both with spiral reinforcement of the concrete core, and without reinforcement, perceiving a short-term compressive load. The aim was studying the strength and features of the stress–strain state of square-section tube-concrete structures samples, made of concrete of classes B40 and B80, taking into account their flexibility.

Nowadays, square-section tube-concrete structures under axial compression have been investigated. 4 series of prototypes were manufactured with cross-sectional dimensions of  $100 \times 100$  mm and a height of 520 mm to solve the experimental set. Metal plates 10 mm thick were welded to the specimens ends. Each series was based on 3 twin samples [1–3].

All samples in one series were cut off from one tube and end-faced. One series was additionally supplied with a frame with spiral reinforcement (Figs. 1, 2). The frame was made of longitudinal reinforcement bars  $\varnothing 6$  A500C (GOST R 52,544-2006) and reinforcing wire  $\varnothing 5$  Bp 500 (GOST 6727-80), which was wound around the longitudinal bars of the frame in a spiral with a pitch of 30 mm. In order to preserve the design shape of the core, the longitudinal and spiral reinforcements were tied with knitting wire. Yield strength of reinforcing wire is A500C  $\sigma_{s,y} = 552$  MPa, Bp500  $\sigma_{s,y} = 548$  MPa. Tensile strength at break, respectively,  $\sigma_{s,u} = 735$  MPa and  $\sigma_{s,u} = 730$  MPa. The spiral winding diameter in the plan was 82 mm. The main samples parameters of each series were as follows: B-45 series - tube-concrete samples made of heavy concrete of class B45, enclosed in a shaped square tube with dimensions  $100 \times 100 \times 4$  mm, height 520 mm, made of steel of class C345; B-80 series - samples similar to the B-45 series, but made of B80 class concrete; series S-80 - specimens similar to series B-80, but made of prestressing concrete of class B80 with a self-stressing value of 2 MPa; SA-80 series - samples similar to the S-80 series, but with a frame with spiral reinforcement.

**Fig. 1** Frames with spiral reinforcement for installation in square-section tube-concrete structures



**Fig. 2** Frames with spiral reinforcement for installation in square-section tube-concrete structures



The following materials were used as components for prototypes manufacturing: portland cement M500 (GOST 10,178-85); sand from the Magnitogorsk sand quarry with a fraction of 0–5 mm; crushed stone from the Beloretsk granite quarry with a fraction of 5–10 mm; superplasticizer Sika «ViscoCrete» 5-600 SP; Ebelit (multi-functional action modifier); electric-welded tubes  $\varnothing 219 \times 5$  mm according to GOST 10,705-80; profile steel tubes  $140 \times 140 \times 4$  mm according to GOST 30,245-2003; fittings A500C  $\varnothing 6$  mm according to GOST R 52,544-2006; fittings Bp500C  $\varnothing 5$  mm according to GOST 6727-80; base plates 10 mm thick made of steel grade St3. The concrete mixture compositions for all the studied series are presented in Tables 1, 2, 3 and 4.

Before the prototypes manufacturing, shell tubes segments of the required dimensions were prepared. Billets of the required length were cut from one shell tube and end-faced on a lathe. For the first series, the initial concrete class B45 of increased strength was adopted. Such concretes are recommended for using a shell tube made of steel grade 09G2S. For the other three series, high-strength concrete is adopted, having a class of axial compressive strength B80.

The technology for manufacturing samples of all series was the same. Initially, a concrete mixture was made to form the structure core. Then, the shell tube with a temporarily installed metal plate, which prevents the concrete mixture from flowing out of the tube, was installed on a vibrating table and securely fastened to it with bolts. Then, gradually, in small parts, the concrete mixture was placed into the tube ( $100 \div 150$  mm each). Self-compacting concrete mixtures were used. At the end of the molding process, the top of the shell tube was covered with a metal plate, similarly to the lower end, in order to avoid shrinkage deformations in the initial stage of the concrete hardening process. The lower and upper typesetting plates were pulled together with steel bands. The sample was moved for 48 h to the area reserved for storage at a temperature of  $20 \pm 3$  °C [4–8].

After two days, the metal plates were removed from the ends, the element ends were cleaned, and end plates 10 mm thick were welded to the shell tube with a continuous seam. All welds were coated with grease to ensure tightness. These activities created favorable conditions for the hardening of the concrete core. The difference in the samples manufacturing of the SA-80 series was that before installing the sample on the vibrating table, a rod frame and wire reinforcement was installed inside the tube (longitudinal - 6 rods  $\varnothing 6$  A500C, ring -  $\varnothing 5$  Bp500). Strain gauges with a base of 5 mm were glued to the longitudinal and spiral frame reinforcement. Control concrete samples in the form of cubes and prisms were made with dimensions of  $100 \times 100 \times 100$  mm and  $100 \times 100 \times 400$  from one batch, in accordance with GOST 10,180-2012. Prior to their stripping, the samples were stored in wet sawdust, excluding moisture evaporation from them, in a room with an air temperature of  $(20 \pm 5)$  °C. After stripping, the control concrete cubes and prisms were stored in accordance with GOST 10,180-2012. The self-tension control of self-stressing concrete was carried out in accordance with GOST 32,803-2014. Concrete self-stress was determined using three control samples-prisms  $100 \times 100 \times 400$  mm in size, molded and hardened in special dynamometric jigs (Fig. 3).

During the concrete expansion, the conductors create an elastic deformations limitation, equivalent to 1% of the longitudinal reinforcement of the prism specimens. Conductors were measured daily for concrete at the age of 1–7 days and further at the age of 10, 14 and 28 days. Each time the measuring device was checked with a



**Fig. 3** Control samples-prisms in conductors

standard (Fig. 4). The measurement results were recorded in the test log for prism specimens in conductors when determining the concrete self-stress. The compressive strength of stress concrete was determined in accordance with the requirements of GOST 10,180-2012. The samples age at the testing time was 30 days. Control samples tests of concrete were performed on an IP-2000 hydraulic press. Electrical strain gauges with a base of 50 mm were used to measure the longitudinal and transverse prisms deformations. The strain gauges readings were recorded using a universal portable multichannel measuring and computing complex MIC-036 (Fig. 5).

The studied samples of square-section tube-concrete structures were tested in a vertical position on a hydraulic press 2PG-500 with a short-term compressive load. The experimental part of the work was carried out using modern equipment and devices certified and metrologically certified. Probabilistic-statistical calculation methods were used to process the array of experimental data obtained. According to the requirements of the current regulatory documents, before the tests, the measurement error assessment by the tensoresistive method was carried out. The features of force resistance revealed in experiments testify to the operation of a concrete core and a steel tube under conditions of a volumetric stress state. Electric strain gauges were used on longitudinal reinforcement with a base of 5 mm and on a shell tube with a base of 20 mm to measure the longitudinal and transverse deformations of



**Fig. 4** Checking the measuring device

**Fig. 5** Measuring and computing complex MIC-036



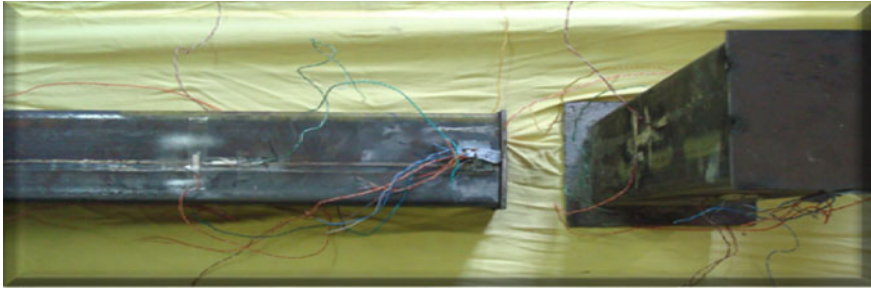


**Fig. 6** Electric strain gauges arrangement on a steel tube-sheath

materials during testing (Fig. 6). The readings of strain gauges were recorded using a universal portable multichannel measuring and computing complex MIC-036. On the shell tube, strain measurements were duplicated by Aistov strain gauges with a scale division of 0.001 mm [9–13].

## 2 The Measurement Error Determination by the Tensorresistive Method

According to the requirements of the current regulatory documents, before the tests, the measurement error assessment by the tensorresistive method was carried out. The error is the difference between the instrument reading and the true measured value:

$$\Delta_{\varepsilon} = \varepsilon_{pr} - \varepsilon_{or} \quad (1)$$

The error depends on the measured deformation level, the measuring device type and the experiment conditions. The tensorresistive method of measuring deformations makes it possible to exclude errors due to voltage fluctuations in the power supply network of the device and the temperature factor. The influence of intrinsic creep of strain gauges is eliminated due to the strain gauges design and the short experiment duration. In this case, the total limiting error of strain measurement is determined by the error associated with the strain sensitivity coefficients  $S$  spread of the strain gauges used and the error  $\varphi$  and  $\varphi_0$  of reading the device and is calculated by the following formulas:

$$\Delta_{\varepsilon} = \sqrt{D_s^2 + D_f^2 + D_{f0}^2} \quad (2)$$

$$\Delta_{\varepsilon} = \frac{\Delta_{\varepsilon}}{\varepsilon} = \frac{1}{\varepsilon} \sqrt{D_s^2 + D_f^2 + D_{f0}^2} \quad (3)$$

$$D_s = \frac{\partial \varepsilon}{\partial S} * \Delta_s = \frac{\Delta_s}{S} * \varepsilon = \overline{\Delta_s} * \varepsilon \tag{4}$$

$D_s$  –partial error due to the spread of the strain gauge factor  $S$ , its value is entered as an average value for a batch of strain gauges;

$D_f, D_{f_0}$ – partial reading errors  $\varphi$  and  $\varphi_0$ .

It was assumed that random measurement errors are subject to the normal distribution law when determining the error. The error estimation of results statistical processing was carried out according to:

$$\overline{\Delta_s} \leq 2\sigma_s \tag{5}$$

where  $\sigma_s = \sqrt{\frac{1}{n-1} \sum_{i=1}^n (S_i + \overline{S})^2}$  – standard deviation  $S$ ;

$n$  – the number of strain gauges in the evaluated batch;

$\overline{S}$  – arithmetic mean value of quantity  $S$ ,

$$S = \frac{1}{n} \sum_{i=1}^n S_i \tag{6}$$

During testing, eight strain gauges were glued onto the steel tube-shell. The strain sensitivity  $S$  of all strain gauges was selected in such a way that it did not differ by more than 0.02 in the selected sensors batch. Then:

$$\sigma_s = \sqrt{\frac{1}{8-1} [(2.10 - 2.12)^2 + (2.11 - 2.12)^2 + \dots + (2.14 - 2.12)^2]} = 0.0214 \tag{7}$$

$$\Delta_s 0.0214 * 2 = 0.0428$$

The partial error  $D_s$  at the deformations level  $1000 \times 10^{-5}$  is:

$$D_s = \Delta_s \varepsilon = 0.0427 * 1000 * 10^{-5} = 42.7 * 10^{-5} \tag{8}$$

Total error:

$$\Delta_\varepsilon = \frac{1}{1000 * 10^{-5}} \sqrt{\quad} \tag{9}$$

or  $\approx 4.3\%$ , which provides the required (no more than 6%) measurement accuracy.

The ends support of the samples was assumed to be hinged. The samples were placed on the press in a vertical position and carefully centered. The axial compressive load was applied for a short time. The load was transferred simultaneously to the concrete core and the steel shell. Since the stress concentration usually manifests itself in the upper and lower end zones, before testing, bandages were fixed at the

**Fig. 7** Mechanical devices scheme during the test for central compression: 1 - dial gauges; 2 - Aistov strain gauges

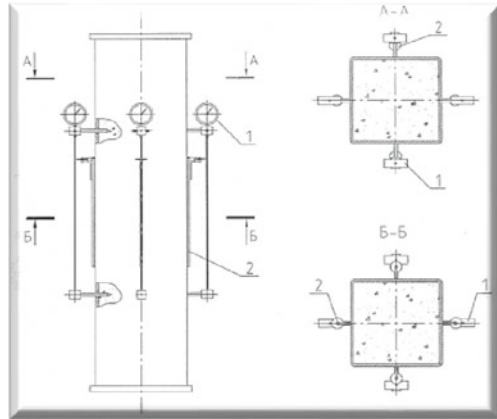


**Fig. 8** General view of the sample during testing



ends of the steel shell tubes in height equal to half the external size of the sample cross section. Mechanical devices scheme during the test for central compression is shown in Fig. 7. General view of the sample during testing is shown in Fig. 8.

### 3 Research Results

In accordance with the requirements of GOST 30,245, GOST 30,432, GOST 32,803, GOST 6727, GOST 52,544 and GOST 10,180, before testing specimens of all columns series, the strength and deformation characteristics of the starting materials were determined. Strips  $400 \times 20$  mm in size were cut from its to determine the mechanical characteristics of the tube steel in tension walls. The destruction nature of steel strips samples is shown in Fig. 9. The mechanical tests results of steel tubes are shown in Table 5.



**Fig. 9** Test result of steel strip samples

**Table 1** The concrete mixture composition for samples of the B-45 series

Material name	Quantity per 1 m <sup>3</sup>
Cement, kg/m <sup>3</sup>	443
Sand, kg/m <sup>3</sup>	704
Crushed stone, kg/m <sup>3</sup>	945
Embelite, kg/m <sup>3</sup>	-
Sika «ViscoCrete», l/m <sup>3</sup>	6.65
Water, l/m <sup>3</sup>	177
W/C	0.4

**Table 2** The concrete mixture composition for samples of the B-80 series

Material name	Quantity per 1 m <sup>3</sup>
Cement, kg/m <sup>3</sup>	465
Sand, kg/m <sup>3</sup>	714
Crushed stone, kg/m <sup>3</sup>	936
Embelite, kg/m <sup>3</sup>	-
Sika «ViscoCrete», l/m <sup>3</sup>	7.0
Water, l/m <sup>3</sup>	167
W/C	0.36

**Table 3** The concrete mixture composition for samples of the S-80 series

Material name	Quantity per 1 m <sup>3</sup>
Cement, kg/m <sup>3</sup>	465
Sand, kg/m <sup>3</sup>	688
Crushed stone, kg/m <sup>3</sup>	912
Embelite, kg/m <sup>3</sup>	93
Sika «ViscoCrete», l/m <sup>3</sup>	9.0
Water, l/m <sup>3</sup>	167
W/C	0.36

**Table 4** The concrete mixture composition for samples of the SA-80 series

Material name	Quantity per 1 m <sup>3</sup>
Cement, kg/m <sup>3</sup>	465
Sand, kg/m <sup>3</sup>	688
Crushed stone, kg/m <sup>3</sup>	912
Embelite, kg/m <sup>3</sup>	93
Sika «ViscoCrete», l/m <sup>3</sup>	9.0
Water, l/m <sup>3</sup>	167
W/C	0.36

**Table 5** The mechanical tests results of steel tubes

Sample type	Quantity, pcs	Yield strength $\sigma_y$ , MPa	Tensile strength $\sigma_u$ , MPa	Elasticity modulus $E_s$ , MPa
Steel strip with a section of 20 × 4 mm	5	372	520	$2.05 \times 10^5$

**Table 6** The mechanical tests results of steel tubes

Series	R, MPa	R <sub>bu</sub> , MPa	E <sub>b</sub> , MPa
B-45	60.1	48,1	38,410
B-80	91.7	82,1	42,545
S-80	94.2	84,5	42,830
SA-80	93.2	83,9	41,750

The test results of concrete control samples are shown in Table 6. The following designations are used here:

$R$  – cubic compressive strength of the original concrete;

$R_{bu}$  – prismatic compressive strength of the original concrete;

$E_b$  – initial modulus of concrete elasticity.

The materials strength characteristics were used to determine the expected breaking load  $N_u$  and to assign the load step value of square-section tube-concrete laboratory samples. The samples were loaded in steps of 5–10% from  $N_u$  up to  $0.7 N_u$ . Further, at  $N_u$  more than  $0.7 N_u$ , the loads were loaded in steps of  $0.05 N_u$  until the compressive load began to drop. During the 10-min exposure at each stage, the readings of all measuring instruments and sensors were recorded. The main results of testing samples of square-section tube-concrete structures are presented in Table 7. Here, the prism strength values of the initial concrete  $R$  and the concrete self-stress values  $P$  are given. The average yield strength of steel  $\sigma$  of profile tubes is assumed to be 372 MPa for all samples. Table 7 shows the experimental breaking loads  $N_u^{exp}$  and the forces  $N_{bp}^{th}$  equal to the sum of the maximum forces in the concrete (reinforced concrete) core and steel shell assuming their work in uniaxial compression [14–24].

**Table 7** The main results of testing samples of square-section tube-concrete structures

Series, sample	R, MPa	P, MPa	$N_u^{exp}$ , kN	$N_b^{th}$ , kN	$N_{bp}^{th}$ , kN	$n_b = \frac{N_b^{th}}{N_{bp}^{th}}$	$k = \frac{N_u^{exp}}{N_{bp}^{th}}$
B-45-1	48.1	0	867	372	779	0.48	1.11
B-45-2	48.1	0	867	372	779	0.48	1.11
B-45-3	48.1	0	900	372	779	0.48	1.15
B-80-1	82.1	0	1100	636	1042	0.61	1.05
B-80-2	82.1	0	1150	636	1042	0.61	1.10
B-80-3	82.1	0	1163	636	1042	0.61	1.11
S-80-1	84.5	2	1200	654	1060	0.62	1.13
S-80-2	84.5	2	1220	654	1060	0.62	1.15
S-80-3	84.5	2	1200	654	1060	0.62	1.13
SA-80-1	83.9	2	1450	650	1116	0.58	1.30
SA-80-2	83.9	2	1480	650	1116	0.58	1.33
SA-80-3	83.9	2	1480	650	1116	0.58	1.33
Mean							1.11

The quantitative assessment of indirect reinforcement influence, due to the restraining effect of the steel tube and spiral reinforcement (if any) is made using the coefficient  $k = N_u^{exp} / N_{bp}^{th}$ . The results obtained indicate that in all four series there is the indirect reinforcement effect. The samples strength turned out to be noticeably higher than the sum of the maximum forces in the concrete (reinforced concrete) core and steel shell, assuming their work in uniaxial compression. The average value of the coefficient k was:

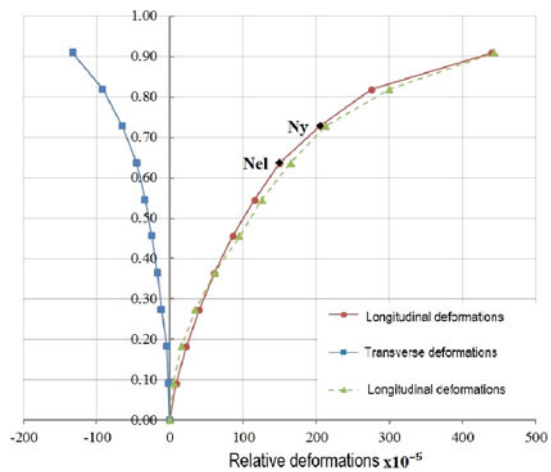
- 12.3% for samples of the B-45 series;
- 8.7% for samples of the B-80 series;
- 13.3% for samples of the S-80 series;
- 32% for samples of the SA-80 series.

The obtained values of the coefficient k confirm the well-known fact that with an increase in the strength of the original concrete, the effect of indirect reinforcement decreases. At the same time, the positive effect of prestressing concrete precompression in samples of the S-80 series is clearly visible. This circumstance should be taken into account when designing square-section tube-concrete structures. The indirect reinforcement effectiveness was affected by the spiral reinforcement presence to an even greater extent. The coefficient k here turned out to be of the same order as in the centrally compressed tube-concrete elements of a circular cross section. At the same time, it is obvious that in cases of eccentric compression, a square tube can be more efficient than a circular one. According to the measuring results of the sample deformations, the dependencies «n-ε» were constructed, where n is the relative value of the compressive load  $n = N / N_u^{exp}$ ; ε is the relative deformation of

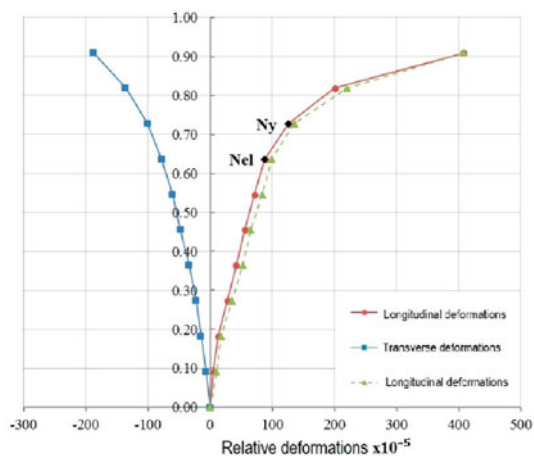
the sample (positive values are axial shortening deformations, negative values are transverse elongation deformations). Characteristic dependencies  $\langle n-\varepsilon \rangle$  are shown in Figs. 10–13. According to these dependencies, it can be seen that the axial deformations of specimens without helical reinforcement already at the loading level  $n = 0.85 \div 0.9$  amounted to  $0.0038 \dots 0.0045$ . Significant plastic deformations developed with a further increase in the load. The concrete core and the steel tube deformed together. Therefore, it can be concluded that the ultimate deformability of the concrete core is significantly higher compared to the deformability of uniaxially compressed concrete.

In specimens of the SA-80 series with helical reinforcement, axial deformations reached about 1.4–1.5% by the failure time. It was revealed that additional indirect reinforcement in the form of a spiral significantly increases the limiting deformations

**Fig. 10** Characteristic dependence  $\langle n-\varepsilon \rangle$  for samples of the B-45 series



**Fig. 11** Characteristic dependence  $\langle n-\varepsilon \rangle$  for samples of the B-80 series



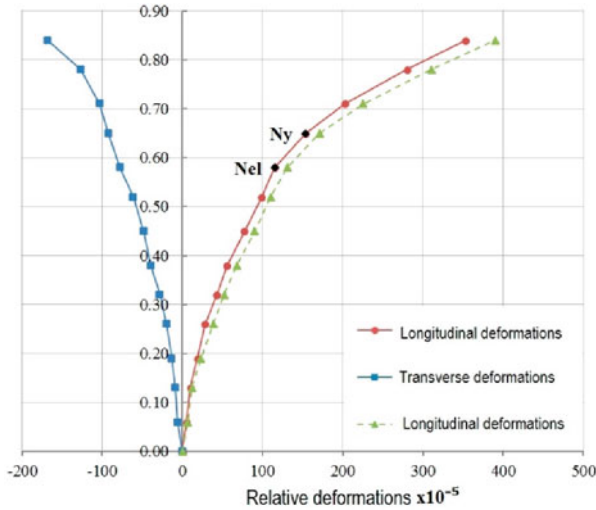


Fig. 12 Characteristic dependence «n-ε» for samples of the S-80 series

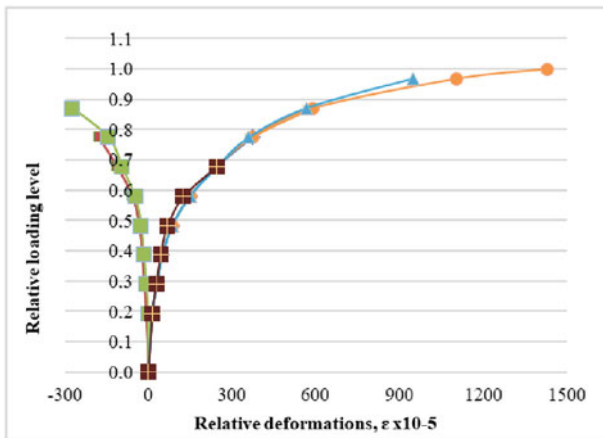


Fig. 13 Characteristic dependence «n-ε» for samples of the SA-80 series

of tube concrete samples. According to these dependences, it can be determined that the elastic work limit of the elements was achieved at loads equal to  $(0.58 \dots 0.65) N_u$ . For samples made of prestressing concrete, the elastic work limit was slightly higher compared to other samples. At the same time, for all samples, axial shortening deformations were much less than the limiting ones and amounted to the order of  $\epsilon_{el} = 110 \times 10^{-5} \dots \epsilon_{el} = 155 \times 10^{-5}$ .

Analyzing the dependencies presented in Figs. 3, 4, 5 and 6 the following features can be noted of the outer steel shell, reinforcing cage and concrete core in the studied

samples. The entire process of power resistance can be conditionally divided into three stages. The first is the quasi-elastic element work. In samples of the SA-80 series, spiral reinforcement is practically not included in the work. The relative elongation strains of the helix did not exceed  $64 \times 10^{-5}$ . The elastic–plastic stage comes next. Here, microcracks begin to form in the concrete core, which contributes to an increase in its volume. The steel tube-shell gradually changes into a fluid state. By the end of this stage, the stresses in the concrete core reach the upper cracking limit. In samples of the SA-80 series, the stresses in the longitudinal reinforcement at this stage do not exceed 60% of the yield strength. Spiral reinforcement is actively included in the work. The presence of indirect reinforcement in the concrete core inhibits the intense microcracks formation. In samples with tension concrete, the the upper and lower boundaries of crack formation become higher. The longitudinal reinforcement of the frame (if any) works practically in conjunction with concrete.

The last work stage is plastic in nature. In the longitudinal and transverse directions, there is a sharp increase in the element deformation. The stresses in the longitudinal reinforcement reach the yield point. In helical reinforcement, the stresses also reach the yield point. A further increase in the load became impossible due to a sharp increase in deformations. Despite the high-strength concrete use in most samples, the destruction nature has always been plastic. At the moment of destruction, folds formed on all side faces of the samples at approximately the same element height. Local buckling of the steel tube was observed, which was more pronounced in the middle zones of the side faces. The concrete was crushed in places where the folds were formed. End plates were removed from some of the samples after testing. Then their steel tube-shell was cut in the vertical direction. The samples destruction nature with a view of the steel tube-shell and the exposed reinforced concrete core are shown in Fig. 14.

The shell tube was difficult to separate from the concrete core. The adhesion was so high that pieces of concrete were removed from the steel shell in elements with



**Fig. 14** Samples view of the SA-80 series after destruction: **a** - the formation of a fold on the shell side surface; **b** - spiral rupture

self-stressing concrete and the spiral frame. It turned out that in all the examined samples, the corrugations formed on the steel tube as a result of the loss of local stability were filled with crushed concrete. A rupture of helical reinforcement was found in the places where corrugations are formed and concrete is crushed in a sample of the SA-80 series. The absence or presence of a spiral frame in steel-tube concrete samples significantly affects its behavior in the limit state stage. The limiting axial strains in specimens with helical reinforcement increased by about 2 times compared with specimens strains of other series.

At the same time, the average strength of SA-80 samples series turned out to be 22% higher compared to analogue samples without spiral reinforcement of the S-80 series. This fact is due to an increase in lateral pressure on the concrete core due to additional indirect reinforcement. The SA-80 and B-45 samples strengths comparison indicates that the central compressive strength of the improved design of square-section tube-concrete structures turned out to be 67% higher compared to traditionally used concrete pipe elements.

## 4 Conclusion

The features of force resistance revealed in experiments testify to the operation of a concrete core and a steel tube under conditions of a volumetric stress state. The deformation nature of the steel tube suggests that its walls experience not only compression in the axial direction. Stretching and bending of the walls from the lateral pressure of the concrete core is also observed. Thus, the tube contribution to the perception of the force  $N_u^{\text{exp}}$  is significantly less than it would be in the assumption of its operation in uniaxial compression. It indicates a noticeably greater contribution of concrete to the perception of the force  $N_u^{\text{exp}}$  in comparison with the conditions of uniaxial compression. The main conclusion of the experiments follows from it. It is advisable to increase the strength of square-section tube-concrete structures by using high-strength concrete and providing more effective indirect reinforcement for it. The power resistance features of square-section tube-concrete structures revealed in the experiments must be taken into account when calculating their strength.

## References

1. Alhatmey, I.A., Ekmekyapar, T., Alrebeh, S.K.: Residual strength capacity of fire-exposed circular concrete-filled steel tube stub columns. *Adv. Concrete Constr.* **6**(5), 485–507 (2018)
2. Ekmekyapar, T., Alhatmey, I.A.H.: Post-fire resistance of internally ring stiffened high performance concrete filled steel tube columns. *Eng. Struct.* **183**, 375–388 (2019)
3. Han, L.H., Wei, L., Reidar, B.: Developments and advanced applications of concrete-filled steel tubular (CFST) structures members. *J. Constr. Steel Res.* **100**, 211–228 (2019)
4. Hassanein, M.F., Patel, V.I., Elchalakani, M., Thai, T.-H.: Finite element analysis of large diameter high strength octagonal CFST short columns. *ThinWalled Struct.* **123**, 467–482 (2018)

5. Hossain, K.M.A., Chu, K.: Confinement of six different concretes in CFST columns having different shapes and slenderness. *Int. J. Adv. Struct. Eng.* **11**, 255–270 (2019)
6. Krishan, A., Rimshin, V., Troshkina, E.: Experimental research of the strength of compressed concrete filled steel tube elements. *Adv. Intell. Syst. Comput.* **1116**, 560–566 (2020)
7. Krishan, A.L., Narkevich, M.Y., Sagadatov, A.I.: Compressed tube-concrete elements with the high-strength compression core and with fibreglass shell. *IOP Conf. Ser. Mater. Sci. Eng.* **687**(3), 033016 (2019)
8. Krishan, A.L., Narkevich, M.Yu., Sagadatov, A.I., Rimshin, V.I.: The strength of short compressed concrete elements in a fiberglass shell magazine of Civil Eng. **94**(2), 3–10 (2020)
9. Krishan, A.L., Rimshin, V.I., Shubin, I.L., Astafeva, M.A., Stupak, A.A.: Compressed reinforced concrete elements bearing capacity of various flexibility. In: Vatin, N., Roshchina, S., Serdjuk, D. (eds.) *Proceedings of MPCPE 2021. LNCE*, vol. 182, pp. 283–291. Springer, Cham (2022). [https://doi.org/10.1007/978-3-030-85236-8\\_26](https://doi.org/10.1007/978-3-030-85236-8_26)
10. Krishan, A.L., Rimshin, V.I., Troshkina, E.A.: Compressed and bending concrete elements with confinement reinforcement meshes. *IOP Conf. Ser. Mater. Sci. Eng.* **753**(2), 022052 (2020)
11. Martinov, V., Lukin, M., Rimshin, V., Rusak, K., Ivaniuk, A.: 2022 Influence of different types of aggregates on the structural properties of fiber-reinforced concrete. In: Manakov, A., Edigarian, A. (eds.) *International Scientific Siberian Transport Forum TransSiberia - 2021 TransSiberia 2021, LNNS*, vol. 403, pp. 1467–1476. Springer, Cham (2021). [https://doi.org/10.1007/978-3-030-96383-5\\_164](https://doi.org/10.1007/978-3-030-96383-5_164)
12. Neverov, A.N., Truntov, P.S., Ketsko, E.S., Rimshin, V.I.: Calculating the strengthening of construction structures before the reconstruction of the building. In: Vatin, N., Roshchina, S., Serdjuk, D. (eds.) *Proceedings of MPCPE 2021 Selected Papers, Lecture Notes in Civil Engineering, LNCE*, vol. 182, 173–179. Springer, Cham (2022). [https://doi.org/10.1007/978-3-030-85236-8\\_14](https://doi.org/10.1007/978-3-030-85236-8_14)
13. Rimshin, V.I., Kalaydo, A.V., Semenova, M.N., Bykov, G.S.: Regularities research of radon transfer to underground enclosing buildings structures. *IOP Conf. Ser. Mater. Sci. Eng.* **953**(1), 012088 (2020)
14. Rimshin, V.I., Roshchina, S.I., Ketsko, E.S., Truntov, P.S., Kuzina, I.S.: Engineering calculations of acidifier retaining walls during water treatment facilities designing. In: Vatin, N., Roshchina, S., Serdjuk, S. (eds.) *Proceedings of MPCPE 2021 Selected Papers Lecture Notes in Civil Engineering, LNCE*, vol. 182, pp. 55–73. Springer, Cham (2022). [https://doi.org/10.1007/978-3-030-85236-8\\_5](https://doi.org/10.1007/978-3-030-85236-8_5)
15. Rush, D.I., Bisby, L.A., Jowsey, A., Lane, B.: Residual capacity of fire-exposed concrete-filled steel hollow section columns. *Eng. Struct.* **100**, 550–563 (2015)
16. Telichenko, V., Rimshin, V., Ketsko, E.: Reinforced concrete structures stress-strain state strengthen with composite materials. *IOP Conf. Ser. Mater. Sci. Eng.* **869**(5), 052003 (2020)
17. Xu, L., Zhou, P., Chi, Y., Huang, L., Ye, J., Yu, M.: Performance of the high strength self-stressing and self compacting concrete-filled steel tube columns subjected to the uniaxial compression. *Int. J. Civil Eng.* **16**(9), 1069–1083 (2018)
18. Kuzina, E., Rimshin, V.: Strengthening of concrete beams with the use of carbon fiber. In: *Adv. Intell. Syst. Comput.* **983**, 911–919 (2019)
19. Varlamov, A.A., Rimshin, V.I., Tverskoi, S.Y.: Planning and management of urban environment using the models of degradation theory. *IOP Conf. Ser. Earth Environ. Sci.* **177**(1), 012040 (2018)
20. Rimshin, V., Labudin, B., Morozov, V., Kazarian, A., Kazaryan, V.: Calculation of shear stability of conjugation of the main pillars with the foundation in wooden frame buildings. *Adv. Intell. Syst. Comput.* **983**, 867–876 (2019)
21. Rimshin, V.I., Varlamov, A.A.: Three-dimensional model of elastic behavior of the composite *Izvestiya Vysshikh Uchebnykh Zavedenii, Seriya Tekhnologiya Tekstil'noi Promyshlennosti* **375**(3), 63–68 (2018)
22. Varlamov, A., Rimshin, V., Tverskoi, S. A method for assessing the stress-strain state of reinforced concrete structures E3S. *Web Conf.* **91**, 02046 (2019)

23. Krishan, A.L., Rimshin, V.I., Troshkina, E.A.: Strength of short concrete filled steel tube columns of annular cross section. IOP Conf. Ser. Mater. Sci. Eng. **463**(2), 022062 (2018)
24. Krishan, A.L., Rimshin, V.I., Astafeva, M.A.: Deformability of a volume-compressed concrete. IOP Conf. Ser. Mater. Sci. Eng. **463**(2), 022063 (2018)